JOURNAL OF MATERIALS SCIENCE 19 (1984) 1159–1170

Microhardness and brittle fracture of garnet single crystals

M. PARDAVI-HORVÁTH
Central Research Institute for Physics, H-1525 Budapest 114, POB 49, Hungary

Hardness and fracture toughness were measured using the Vickers microhardness test in the low load range from 25 to 100 g near to the fracture threshold for near-perfect single crystals of garnets. The influence of crystal growth parameters, calcium impurity content and crystallographic orientation of $Gd_3Ga_5O_{12}$ (GGG) and $Ca_3Ga_2Ge_3O_{12}$ (CaGeGG) samples was investigated. Fracture starts with radial cracking from indent corners followed by lateral fracture of two distinct modes. The mean hardness of [1 1 1] oriented GGG is $H = 13$ GN m^{-2}, for [1 1 1] oriented CaGeGG it is 12 GN m^{-2}, the average fracture toughness being $K_c = 1.2$ and 0.8 MN m$^{-3/2}$, respectively for the two crystals. Impurity doping slightly increases the strength of the material. Among the investigated crystals (1 1 1) faces are the least strong, the (1 0 0) face has maximum H and K_c values for CaGeGG. The constraint factor, ϕ, and yield stress, Y, were deduced from the measured hardness data, giving $\phi = 2.2$ and Y about 7 GN m^{-2}.

1. Introduction

Garnets are ionic crystals with cubic crystal structure of a general formula $A_3B_5O_{12}$. The elementary cell contains 8 formula units with 160 ions. The cations fill three different kinds of sites inside oxygen ion polyhedra. The crystal structure is loose enough to make possible the substitution of cations in a wide range of valencies and ionic radii. In consequence, materials with predetermined properties can be tailored from garnets.

Naturally occurring garnets are minerals, isomorphous mixed silicates and they are used as gemstones. Their Moh's hardness is in the range 7 to 7.5, compared with 8 for spinels and 9 for sapphire (corundum). It is known from jeweller's practice that they are brittle with no definite cleavage planes.

Synthetic garnets of composition $R_3M_5O_{12}$, where R denotes a rare earth ion and M is a metal cation, are widely used as materials for microwave devices ($Y_3Fe_5O_{12}$ = YIG), laser host crystals ($Y_3Al_5O_{12}$ = YAG) and magnetic storage materials in bubble memory devices (epitaxial layers of substituted YIG). For bubble memory and integrated device application a thin garnet film is needed that can be grown epitaxially on a single crystalline substrate with the same crystal structure and lattice parameter. $Gd_3Ga_5O_{12}$ (GGG) is the most widely used substrate material, along with other, less expensive candidates like $Ca_3Ga_2Ge_3O_{12}$ (CaGeGG).

GGG crystals are grown as boules of 2 or 3 inch diameter from the melt at about 2000 K by the Czochralski method, then sliced by a diamond saw, lapped and finally polished chemico-mechanically to obtain a perfect, featureless, flaw-free, near-atomically smooth surface. These crystals are practically defect-free, having dislocation and inclusion densities below 10 cm^{-2} [1].

However, one of the most serious problems during GGG growth, substrate machining, and wafer dicing is the cracking and/or breaking of the crystals. In view of this, it is surprising that no systematic study seems to have been published regarding the mechanical properties of garnets.

Heinz *et al.* [2] published data on the physical properties of $Dy_3Ga_5O_{12}$ and GGG crystals together with the hardness values of 13.50 and 12.50 GN m^{-2} for DyGG and GGG, respectively.

0022–2461/84 $03.00 + .12

Measurements were made at 300 g load, with an error of 35%. Ehman [3] investigated the work damage during surface preparation of crystals, important as substrates for microelectronic devices. For (1 1 1) oriented GGG he measured a Knoop microhardness of 1098. Details of the measurement were not given.

The aim of our work was to study the hardness and fracture characteristics of nonmagnetic garnet single crystals in dependence of the conditions of growth, impurity content and crystallographic orientation. Knowledge of these parameters seems to be very important not only for machining such crystals, but for preventing fracture during growth and device fabrication. At the same time these garnets are good model materials for brittle fracture theory, as they are single crystals of cubic crystal structure, they are elastically isotropic, homogeneous, without internal defects (dislocations, inclusions, flaws) their surface is atomically smooth, and massive samples can be investigated. These crystals are colourless and transparent in visible light, making visual, microscopic observation very easy. As a consequence, simplifying assumptions and approximations of the theory can be proved and approved in this case.

2. Experiments

The investigated crystals were grown by the Czochralski method, with a fully automatized diameter control, along the [1 1 1] crystallographic direction.

Three groups of crystals were investigated.

Group A: $Gd_3Ga_5O_{12}$ crystals, each grown under slightly different conditions (A4 was cracked during cooling).

Group B: calcium doped GGG. Doping with calcium changes the front of crystallization and drastically reduces the number of dislocations via oxygen vacancy formation, already at the lowest level of doping [4]. The calcium content of the melt was 0, 10, 20, 30 ppm for crystals B1 to B4, respectively.

Group C: $Ca_3Ga_2Ge_3O_{12}$ crystals, surfaces parallel to various crystallographic faces.

After growth, boules were cut into wafers, polished and cleaned in accordance with bubble memory device requirements [1]. Growth defects of crystals, as cores, facets, inclusions and dislocations, were measured due to the stress-induced birefringence contrast in the optical microscope between crossed polarizers [1]. The thickness of wafers of groups A and C was 0.5 mm, for group B it was 1 mm. All samples except C1 and C2 had a (1 1 1) oriented surface.

Microhardness measurements with a Vickers indenter were performed in a Neophot-2 microscope (Zeiss, Jena) with an mhp-100 microhardness tester. The maximum applied load was 100 g, above which intensive cracking (conchoidal fracture) occurred. The minimum load (20 g) was above the threshold of radial cracking. Indentation sizes and crack dimensions were measured either at × 1000 using a dry objective of N50 in the same microscope, or at × 1700 from microphotographs. The statistical average and its dispersion were calculated from a minimum of three indentations at each load, taking into account each radial and/or lateral crack length. The curve fitting was done by regression analysis (least squares fit), and the correlation of each fit was calculated.

Measurements were made in air. This can be justified by the simplicity of the experiments; however it is known that ferrites are usually weakened by moisture. Processes connected with grain boundary effects are excluded in our case, but the lowering of surface tension is not. As the indentation depth is above the critical value for creep (see [5]), it is not likely that the results were influenced by this effect.

As garnets have no preferred cleavage planes, the orientation of the indents was accidental, with subsequent indents made along a row, having parallel diagonals on each crystal. Repeated measurements along other directions did not give significantly different results.

The indenter was applied quasi-statically, the loading time was typically 5 to 10 sec. The specimen remained under load for 5 sec, because acoustic emission associated with cracking in accordance with the experiments of Lankford and Davidson [6], occurs immediately upon application of the load. We were not able to decide if radial cracks extended upon unloading, but in some cases abrupt expansion of lateral cracks was observed even 20 to 40 sec after unloading.

3. Results

3.1. Morphology

Indentations from the Vickers pyramid were

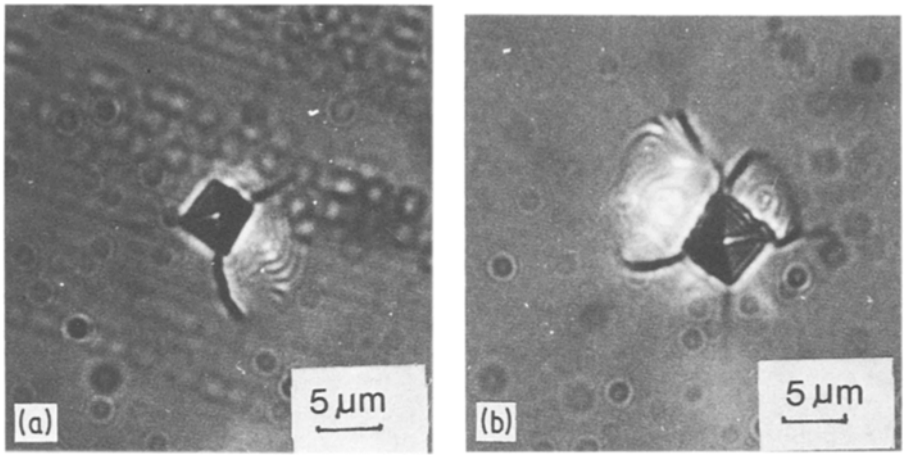

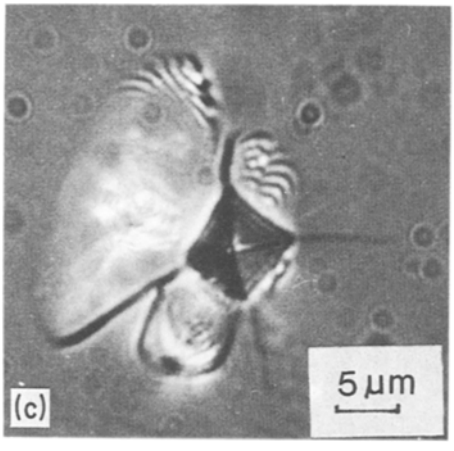

Figure 1 Microphotographs of indentations on the (1 1 1) face of a GGG crystal (sample B1) made at: (a) 25 g, (b) 37.5 g, and (c) 50 g loads.

characteristic of typical hard and brittle materials. Below about 10 g load the indentations were too small to be measured accurately owing to the finite resolution of the optical microscope. Fig. 1 reproduces the microphotographs of the indentations for sample B1, made at increasing load. The minimum load, when the very shallow, faint radial cracks starting from the corners of the indent became "measurable" (i.e. when the length of the radial cracks, c_r, is approximately equal to the indentation diameter $2a$) was in this case 20 g. On increasing the load, radial cracks appear first, followed by developing laterals. At $p = 25$ g distinct radial cracks and faint lateral cracks occur. At higher loads, simultaneously with the extending of the radials, well-developed laterals grow in a way which is characteristic of the whole family of crystals investigated in the present work. Lateral cracks develop as extending parallel conchoidal ridges, connecting the radial cracks at higher loads. Even though determination of the indent diameter (Fig. 1) can be performed with fairly high accuracy (5%), this is not true of the length of radial cracks (c_r); the length is usually underestimated because their very shallow, diminishing ends are not well defined. For laterals (c_l) this is even more valid.

At low loads another type of lateral crack occurred occasionally in GGG (Fig. 2) and regularly in CaGeGG (Fig. 3). These cracks, marked by arrows in Figs. 2 and 3, are originating not from the corners of the indentation but from the middle of its sides, in some cases in pairs on opposite sides of the indentation, as seen in Fig. 3, but Fig. 2 shows the simultaneous appearance of both types. In the following calculations they were treated as laterals, as they occurred in conditions similar to the case of laterals.

All of the GGG crystals show similar indentation patterns; CaGeGG differs from them not so much in average hardness and brittleness, but in the behaviour with respect to various crystallographic planes. Fig. 3 illustrates the indentations on the (1 0 0), (1 1 0) and (1 1 1) faces of CaGeGG crystals at the same load of 50 g. On the (1 0 0) wafer, in addition to the rather short radial cracks, longer, shallow lateral crack lines of the above mentioned type were observed without the usual curved lateral crack configuration. On the (1 1 0) wafer these configurations are pronounced, whereas on the [1 1 1] oriented crystal the contrast in the microscope for lateral cracking is very faint, but extends to a large distance. Fig. 4 shows the same CaGeGG (1 1 1) crystal after loading with

Figure 2 Indentation on the (1 1 1) face of sample B3 at 50 g load. Two distinct modes of lateral cracking (C and M) are visible.

75 g. In this case the impression itself is damaged, the well-developed lateral cracks extend into its interior. For [1 1 1] oriented GGG the typical crack pattern at $p = 100$ g is given in Fig. 5.

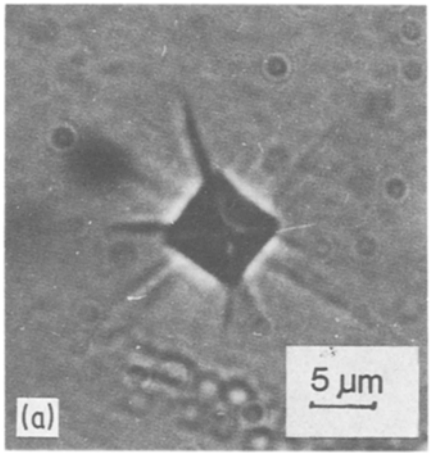

3.2. Hardness

Typical indentation diameters were in the range 6 to 10 μm for loads of 25 to 75 g, respectively. In the applied load range the hardness was independent of the load, where H was evaluated from the measured indentation diameter $2a$ according to the relation

$$H = \frac{0.4636p}{a^2} \qquad (1)$$

Vickers microhardness data are summarized in Table I. The hardness values have a maximum standard deviation of 6%. The maximum difference for various garnets is less than 20%. There is no obvious relationship between the crystal

Figure 3 Indentation morphology at 50 g load on various crystallographic faces of a CaGeGG crystal: (a) (1 0 0), (b) (1 1 0), (c) (1 1 1) faces (samples C1 to C3). Along with extensive radial cracking distinct lateral fracture behaviour is observable.

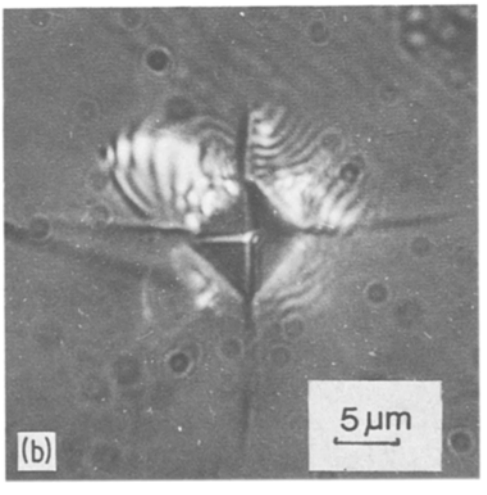

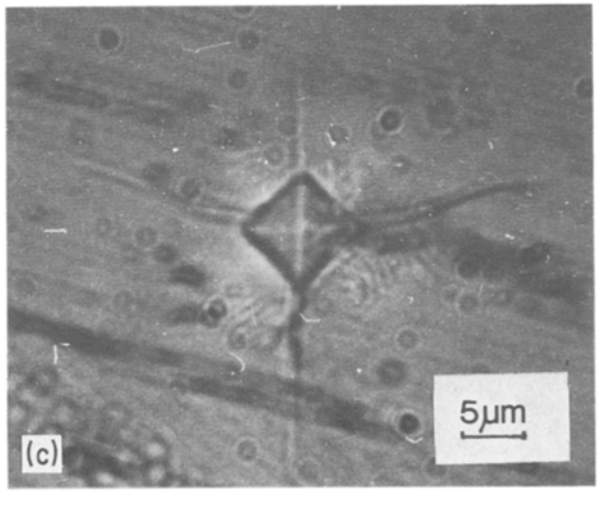

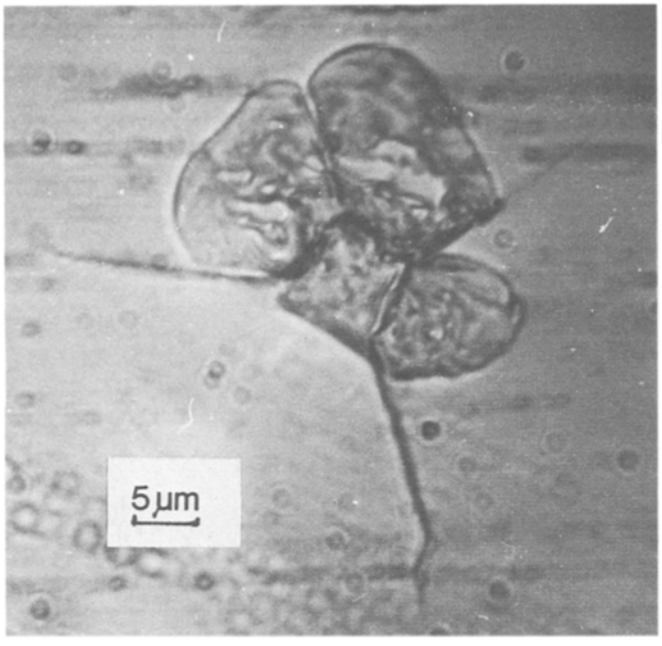

Figure 4 Indentation on C3 sample at 75 g load, where extensive lateral cracking protruding into the indent occurs.

growth conditions, which were not substantially different for group A, and the hardness figures. Crystal A4 contained a stressed central core, and hardness measurements were made on this part, too, giving results within the error limits of unstressed crystals. For calcium-doped group B there seems to be a tendency towards increasing hardness with increasing calcium content. For CaGeGG (group C) the overall hardness is less than that of the GGG. The hardness on the (1 0 0) is the highest, decreasing on the (1 1 0) face, with a minimum on the (1 1 1) wafer.

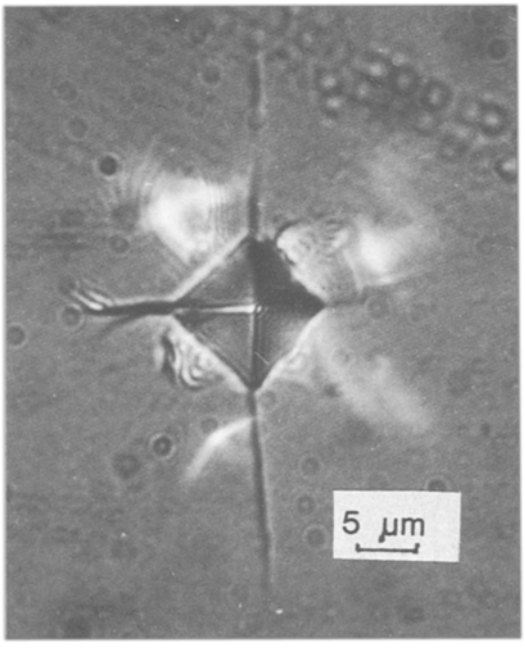

Figure 5 Indentation on the (1 1 1) face of sample A3 at 100 g applied load. In contrast to Fig. 4, extensive lateral cracking has not yet started.

3.3. Crack size

Averaged crack lengths normalized to the impression radius (c/a) are given in Table I. The length of the radial cracks (i.e. indentation-centre–crack-end-distance) emerging from the indentation corners could be determined with the reasonable accuracy of 10% in spite of the sharpness of the tips of the arrested cracks. The length of lateral cracks (c_l) was defined as the distance between the centre of the impression and the most distant point of each lateral crack, averaged for each indentation and load. As not only the length varies over samples, but the intensity (i.e. the sharpness of the contrast) of the cracks, too, as can be seen in Fig. 3, the use of c_l as a parameter for further calculations does not seem very convincing. The higher error of about 20% in the determination of c_l support these arguments.

The load dependence of c_r and c_l can be described by a function of the form $p = Ac^B$ with a single exponent for different crystals:

$$p = A_1 c_r^{(1.37 \pm 0.19)} \quad (2)$$

TABLE I

Material	Orientation	Number	Relative crack length		Hardness, H ($GN\,m^{-2}$)	K_c		ϕ	Y ($GN\,m^{-2}$)
			c_r/a	c_l/a		Eqn 8	Eqn 9		
GGG	[111]	A1	3.14	1.60	12.60	1.02	1.01	2.22	6.0
		A2	2.30	2.60	12.34	1.35	1.62	2.22	6.0
		A3	2.68	1.96	13.02	1.22	1.32	2.16	6.6
		A4	2.78	2.38	13.69	1.19	1.26	2.16	6.6
Ca:GGG	[111]	B1	3.00	2.84	13.25	1.08	1.09	2.16	6.6
		B2	2.91	1.94	13.54	1.17	1.20	2.10	7.0
		B3	2.85	2.41	14.00	1.21	1.26	2.10	7.0
		B4	2.26	2.21	14.15	1.47	1.78	2.10	7.4
CaGeGG	[100]	C1	2.31	0.8	12.72	1.33	1.58	2.0	6.4
	[110]	C2	3.11	2.44	11.60	1.00	1.00	1.9	6.0
	[111]	C3	3.71	3.10	11.49	0.84	0.78	1.9	6.0

and

$$p = A_2 c_l^{(1.02 \pm 0.28)} \quad (3)$$

These relationships between c and p are depicted in Fig. 6. For clarity, not all the measured crystals are included, but fitting involved every data point. Parallel lines on the figures show slopes of the fitted curves. The scatter of data points is much less for radial cracks where the exponent is very near to 3/2. The exponent of the lateral crack function has too wide limits to make any conclusion on its universality.

Evans and Wilshaw [7] showed a consistent relationship between c_r and a for all materials, with a tendency towards larger cracks in harder materials; Fig. 7 gives the results of our measurements. The above indicated tendency is clearly seen; fitting gives the following results:

$$c_r = C_1 a^{(1.20 \pm 0.27)} \quad (4)$$

and

$$c_l = C_2 a^{(1.72 \pm 0.61)} \quad (5)$$

4. Discussion

4.1. Hardness

Hardness values measured for different crystals, given in Table I, are in accordance with previous, approximate results of [2, 3]. The average Vickers microhardness for [111] oriented GGG crystals is $H = 12.98 \pm 0.65\ GN\,m^{-2}$. The error limit is ± 5%, which suggests the basic similarity of GGG crystals, independent of dopant concentration or growth conditions. Table II summarizes literature data together with the results of the present work for some technologically important single crystals. Synthetic garnets, such as GGG and CaGeGG are well-fitted to this series, finding their place according to the classical Moh's hardness formulation. There seems to be a tendency towards higher hardness values with increasing impurity content (calcium doping in group B). The mechanism of this effect is not very clear, although with calcium doping the crystals become more perfect, as the number of dislocations decreases below the origi-

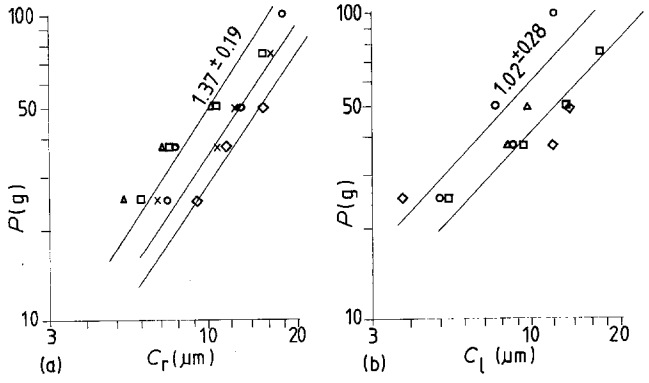

Figure 6 Load dependence of (a) radial crack length, (b) lateral crack length for A2 (□), A3 (○), B2 (X), B3 (△) and C2 (◇) crystals. Lines are for orientation with slopes of the curves fitted to all experimental data.

TABLE II

Material	Orientation	H (GN m^{-2})	E (GN m^{-2})	K_c (MN m$^{-3/2}$)	γ_{calc} (J m^{-2})	σ_{calc} (GN m^{-2})	p^*_{calc} (N)	c^*_{calc} (μm)	Reference
C (diamond)	[111]	84	1210	3.6	5.4	205	0.006	0.08	[14]
Al_2O_3 (corundum)	[0001]	23	460	2.1	4.8	46	0.035	0.37	[12, 14]
$MgAl_2O_4$ (spinel)		16	300	1.7	4.8	69	0.009	0.29	[12]
$Gd_3Ga_5O_{12}$ (garnet)	[111]	13	220	1.2	3.3	49	0.050	0.50	
$Ca_3Ga_2Ge_3O_{12}$	[111]	12	200	0.8	1.6	33	0.004	0.18	
MgO (periclase)	[100]	9	245	1.2	1.2	37	0.06	0.8	[11, 14]

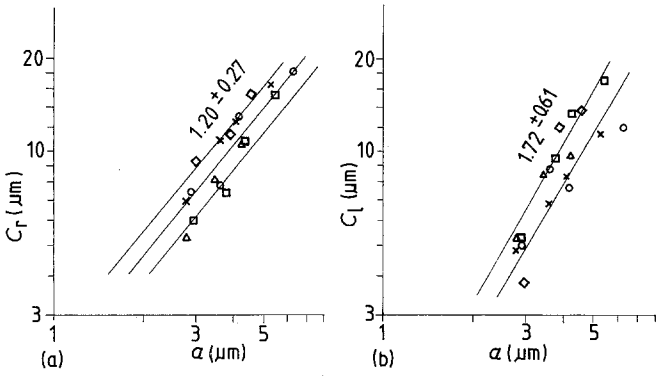

Figure 7 Indent radius as a function of: (a) radial, and (b) lateral crack length. For symbols, see Fig. 6. Slopes of the lines are those of the fitted curves.

nal dislocation density of less than 10^2 cm^{-2} [4], which was already very low. At the same time the decreasing number of dislocations is likely to be accompanied by the growth of point defect concentration.

In-plane orientation dependence has not yet been investigated: repeated measurements along arbitrary directions on a given plane gave no significantly different results.

Results of microhardness measurements on CaGeGG crystals cut along the three basic crystallographic directions of a cubic lattice showed a hardness anisotropy of 10%. The overall hardness is less than that of the GGG, which can be justified by the lower melting point of the CaGeGG. The hardest face is (1 0 0), while the (1 1 0) and (1 1 1) faces have lower, nearly identical hardnesses (see Table I).

The hardness of ionic crystals is influenced by the coordination number of cations, the valence of the ions, and the distance between the ions in the crystal lattice. The garnet structure is complex; it is composed of 24 oxygen tetrahedra, 16 octahedra and 24 dodecahedra with the cations at their centres, while the lattice parameter a is above 12 nm. $Gd_3^{3+}Ga_5^{3+}O_{12}^{2-}$ is a simple garnet with $a = 1.2383$ nm, compared with $a = 1.2322$ nm for $Ca_3^{2+}Ge_3^{4+}Ga_2^{3+}O_{12}^{2-}$. Usually, for isomorphous crystals, lattice parameter decrease leads to increased hardness. In this case, it is likely that the valence differences determine the hardness, which is lower for CaGeGG, as in both GGG and CaGeGG the octahedral sites are occupied by Ga^{3+} cations; the tetrahedral sites in GGG are filled with Ga^{3+}, in CaGeGG with Ge^{4+}.

In the [1 1 1] direction it is relatively easy to penetrate into the crystal because long, non-crossing chains of coordination octahedra are running along this direction. From other directions the garnet lattice looks more dense. These structural peculiarities can lead to hardness anisotropy in spite of the remarkable elastic isotropy [8].

4.2. Crack formation

As was discussed in Section 3.1, crack formation in garnets begins with the occurrence of Palmquist cracks, i.e. shallow, radial surface fractures emerging from the corners of the indentation pit. Once started, they propagate for a given distance, dependent on the material's elastic parameters. This observation is in full accordance with other work [6, 9, 10] on brittle single crystals. At higher loads lateral cracks are formed in a characteristic manner, mainly by conchoidal-like fracture up to the highest loads applied in this work.

The critical load for crack formation depends on the surface finish, decreasing as the surface roughness increases. This factor can be excluded in the case of these garnets with surfaces smooth to some nanometers, without any highly stressed surface layer [1].

Lawn and Evans [11] discussed the possibility of calculating threshold crack size (c^*) and pressure (p^*) for so-called "penny-shaped" median crack formation. They found that hardness and toughness are the controlling parameters in resistance to cracking:

$$c^* \sim (K_c/H)^2 \tag{6}$$

$$p^* \sim (K_c/H)^3 K_c \tag{7}$$

For garnets, c^* and p^* were calculated according to [11]. Table II gives the calculated threshold parameters. GGG values are averaged over the measured samples. Threshold loads in this series are relatively high for GGG and low for CaGeGG of [1 1 1] orientation. As stated above, experimental determination of threshold parameters

from microscopy is uncertain; nevertheless, an attempt was made to compare them with experimental observations. The observed critical loads were about 20 g or slightly below, which gives the upper bound for the threshold.

Lankford and Davidson [6, 9] made precise measurements by the acoustic emission method of the crack-initiation threshold for a range of single crystal materials. These authors found that the experimental threshold loads were below those given by Evans [11], as a consequence of the larger extent of the plastically deformed region beneath the indenter and the difference in tensile stress for subsurface median cracks and surface radial cracks. Their results verify the validity of the method of Lawn and Evans for treating the indentation threshold problem despite the real situation concerning the initiation of radial rather than median cracks. In any case, the ordering of the materials according to the threshold parameters of [11] is correct. The size of threshold cracks is predicted correctly by Equation 6, but these values (of the order of 10^{-1} μm for garnets) are inaccessible to optical microscopy. The very shallow appearance on a perfectly smooth surface also makes their observation difficult by scanning electron microscopy.

4.3. Fracture toughness evaluation

Fracture toughness, or critical stress intensity factor, K_c, is an important material parameter in the application of brittle solids. The most simple method for K_c determination, as was shown by Evans and Wilshaw [7], is based on indent radius and radial crack length measurements in microhardness tests. Evans and Charles [12] showed that microhardness measurements performed in the load range corresponding to the appearance of radial cracks can be fitted to a relationship based on a logarithmic dependence on c_r/a to give K_c:

$$\frac{K_c\phi}{H(a)^{1/2}}\left(\frac{H}{E\phi}\right)^{0.4} = 0.055 \log\left(\frac{8.4}{c_r/a}\right) \quad (8)$$

Knowledge of Young's modulus, E, the constraint factor ϕ, the measured indentation radius, a, and radial crack length, c_r is assumed.

The Young's modulus of GGG was calculated from the elastic constants of [8] leading to $E = 220$ GN m^{-2}. There are no elastic data in the literature for CaGeGG, therefore we used the approximate value of $E = 200$ GN m^{-2}, which can be verified by the lower melting point and structural similarity. The stress to produce plastic flow in a brittle material (Y) can be found from indentation tests [13, 14].

From the measured microhardness and calculated Young's modulus, the constraint factor ϕ was determined according to Marsh [13]. The constraint factor is usually taken as 3, which is valid for an indenter in the form of a flat rigid die penetrating an elastic–plastic material. More realistic values are based on the approximation of the expansion of a hemispherical cavity by an internal pressure of H. For given H/E values ($H/E \simeq 0.06$ for GGG), Y/E can be determined for a known Poisson ration ($\nu = 0.3$ for garnets). Calculated constraint factors and yield stresses (Y) are included in Table I. The ϕ values are below 3, the average being about 2.2 for GGG and 2 for CaGeGG. Yield stresses are of 6 to 7 GN m^{-2}, well below the fracture stress of the material.

The data can be fitted to a more general $(c_r/a)^{-3/2}$ relationship, calculated for well-developed so called "half-penny" type cracks. The exponent $-3/2$ is characteristic of the fracture produced by a central force on wedging a penny-shaped crack of length of $2c_r$. For the present case it is equivalent to the statement that radial Palmqvist cracks from the tip of the indenter are identical to half-penny cracks of length $2c_r$, connected by the plastic zone beneath the indenter [10].

$$\frac{K_c\phi}{H(a)^{1/2}}\left(\frac{H}{E\phi}\right)^{0.4} = 0.129(c_r/a)^{-3/2} \quad (9)$$

Niihara *et al.* [15], to extend the validity of Equation 9 to a lower c_r/a range where radial cracks are formed and definitely not half-pennies, renormalized Evans' data as a function of l/a, where $l = c_r - a$, and fitted to the function

$$\frac{K_c\phi}{H(a)^{1/2}}\left(\frac{H}{E\phi}\right)^{0.4} = 0.035(l/a)^{-1/2} \quad (10)$$

Lankford [16] showed that Niihara's relationship was not universal: the exponent of Equation 10 varies with materials. At the same time, the $(c_r/a)^{-3/2}$ dependence seems to be more universal, and a best-fit curve was proposed in the form

$$\frac{K_c\phi}{H(a)^{1/2}}\left(\frac{H}{E\phi}\right)^{0.4} = 0.142(c_r/a)^{-1.56} \quad (11)$$

which is very close to Equation 9.

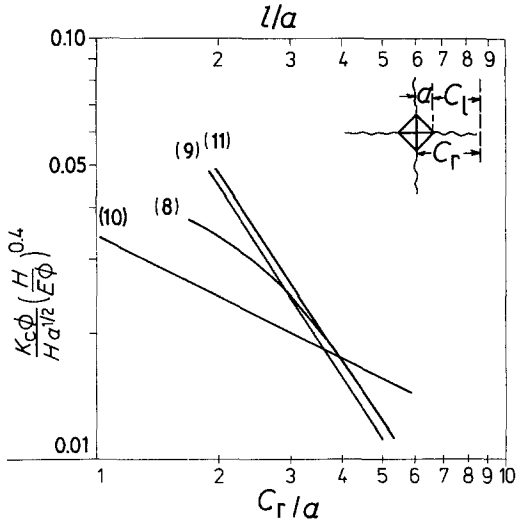

Figure 8 Correlation of normalized fracture toughness/hardness relation with the normalized radial crack length according to various models (Equations 8 to 11). Each curve has the number of the corresponding equation (see text).

Replotted functions of Equations 8 to 11 are given in Fig. 8. In the load range of our experiments (25 to 100 g), c_r/a average values were between 2.3 and 3.8 (see Table I). If c_r/a is larger than 2.5, Equations 8, 9 and 11 give results for K_c differing by a maximum of 15%. Equation 10 gives nearly the same K_c in the range of $3.5 \leqslant c_r/a \leqslant 4.5$, taking into account experimental uncertainties, but deviates in the low crack length range.

According to Lankford [16], K_c evaluation from the indentation method, if E and ϕ are known, is valid with an error of 35%. Our experience shows that K_c values can be determined more precisely from indentation in the range $2.5 \leqslant c_r/a \leqslant 5$.

In the present work K_c was calculated from Equation 9, as the argumentation in favour of the $-3/2$ dependence seems most convincing. For crack sizes below $c_r/a \leqslant 2.5$ deviations became more significant, although K_c can be calculated in 15% error limits. Standard deviations of 10% in c/a measurements, due to the indefinite crack arrest points, give K_c within the same error limits. We can conclude that the accuracy of K_c determination is limited by the error of c/a measurement, independent of the physical picture and validity of Equations 8 to 11. K_c values deduced from the Blendell logarithmic fit of Evans' data [4] and the Evans–Lankford $-3/2$ dependence are given in Table I.

Fracture toughness values are summarized in Table I. Table II compares K_c of single crystals, among which garnets have found their place in accordance with their hardness and Young's moduli. The average fracture toughness for [1 1 1] oriented GGG crystals, including the calcium doped series is 1.32 ± 0.24 and there is some indication of increasing K_c with increasing calcium doping in Group 2 crystals. For CaGeGG the most easily cracked plane is (1 1 1), with $K_c = 0.78$, half that measured in the (1 0 0) plane.

Evans and Wilshaw [7] obtained for $c/a > 2$ a relationship for the relative size of lateral and radial crack lengths

$$c_l/c_r \sim (pH/K_c^2)^{1/4} \qquad (12)$$

which was proved for [1 1 1] oriented garnets. CaGeGG wafers are not included as the lateral crack initiation threshold was very near to 25 g. Our data were fitted to Equation 12 and a linear relationship was obtained

$$(pH/K_c^2)^{1/4} = 0.284 - 0.095(c_l/c_r) \qquad p = 25\ \text{g} \qquad (13)$$

with the correlation factor $r = 0.88$. Although the correlation is not exact, K_c can be estimated from c_r and c_l measurements, too.

From K_c the fracture surface energy of the solid, γ, can be determined from

$$\gamma = \frac{K_c^2}{2E} \qquad (14)$$

thereby providing an approximation for the breaking strength or cleavage stress of the material. For perfect crystals the latter is assumed to be equal to the cohesive strength

$$\sigma = (E\gamma/a_0) \qquad (15)$$

where a_0 is the intermolecular distance. From Equations 14 and 15 the theoretical cohesive strength of GGG is about $0.2E$, much higher than the yield stress of $0.03E$, which means that flow can play a definite role in the fracture of garnets. Values of surface energies and cohesive forces are shown in Table II, and confirm the large values expected for these materials. For other crystals in the table, γ and σ were also calculated according to Equations 14 and 15. These data can be very useful in practical applications in optimizing technological processes which involve the wetting of surfaces by liquids, as in cutting, polishing, and above all, cleaning procedures.

5. Conclusions

Microhardness tests by a Vickers indenter were performed on practically defect-free, single crystalline $Gd_3Ga_5O_{12}$ (GGG) and $Ca_3Ga_2Ge_3O_{12}$ (CaGeGG) samples. The average hardness value for pure and calcium-doped GGG crystals with [1 1 1] surface normals is 13 GN m^{-2}. There is a tendency towards increasing H with increasing calcium content from 13.25 to 14.15 GN m^{-2} in the 0 to 30 ppm calcium range. CaGeGG samples were cut normal to [1 0 0], [1 1 0] and [1 1 1] crystallographic directions. The maximum hardness was obtained on (1 0 0) crystals, while the (1 1 1) wafer has the minimum hardness.

Experiments were performed in the low load regime in order to prevent significant rupture of the brittle crystals, and to investigate the crack initiation processes near the threshold, at low crack-to-indent ratios ($c/a < 5$). It was established that the first cracks extending from the corners of the indenter are Palmqvist-type radial cracks, rather than median cracks, in accordance with Lankford's [16] observations. Nevertheless, the Evans–Charles relationship [12] for fracture toughness determination from indentation and crack sizes with the $-3/2$ exponent is found to be valid, as radial cracks can be treated as two halves of a half-penny crack connected by the indentation plastic zone.

The threshold loads and crack length given in Table II was calculated according to the Lawn–Evans [11] and the Lankford–Davidson [6] model for a group of single crystals, giving $c^* = 0.5$ μm for the critical dimension of a crack in GGG which can grow if loads in excess of $p^* = 5$ g are applied. For (1 1 1) oriented CaGeGG, p^* is an order of magnitude lower.

Lateral cracks are usually of conchoidal type, and tend to expand even after unloading. Lateral fracture is an important mode of material removal by abrasive processes. The morphology of the laterals is especially important, as conchoidal fracture is preferred during the lapping and grinding operation.

Fracture toughness was determined according to [12], its mean value for (1 1 1) oriented GGG being 1.3 MN m$^{-3/2}$, increasing slightly with calcium doping and depending on crystallographic orientation; the (1 0 0) plane of CaGeGG crystal has the highest fracture toughness. The relative value of the lateral and radial crack lengths (c_l/c_r) can yield the approximate value for K_c [7] given by Equation 13.

From microhardness measurements the yield stress of a brittle material can be determined [13], the value of this being 6.6 GN m^{-2} for garnets, i.e. of the order of $0.03E$. From the fracture toughness, the surface energy and the cleavage stress (i.e. the theoretical strength) can be deduced, the latter being about $0.2E$.

Hardness and fracture toughness together determine the rate of material removal by cutting and lapping steps of GGG substrate machining. During the performance of these processes cracking has to be eliminated, as it is the most troublesome defect in brittle crystal machining. Handling damage, the other main source of production yield decrease, usually originates from contact with particles, reminiscent of the sharp indenter configuration in microhardness tests. The wetting of crystals during cleaning and machining is indirectly connected with fracture toughness through surface energy changes.

In consequence, a knowledge of these parameters for brittle oxide single crystals, which are of immense important for microelectronics, is indispensable and has a direct influence on the optimization of the technological processes. On the other hand, garnet crystals can be grown with highly controlled, "tailored" properties, in wide limits of composition and lattice parameter, with the practical possibility of substituting any garnet-forming ion for other types of different valence and ionic radius. In this way it is possible to gain insight into the effect of the change in chemical bonding and site preference on macroscopic mechanical properties. Near perfect quality, isotropy, and transparency, make garnets attractive candidates for future work on brittle solids.

Acknowledgement

The author is very grateful to Drs J. Paitz and L. Gosztonyi for the samples and stimulating discussions.

References

1. M. PARDAVI-HORVÁTH, *Progr. Cryst. Growth Charact.* 5 (1982) 175.
2. D. M. HEINZ, L. A. MOUDY, P. E. ELKINS and D. J. KLEIN, *J. Electron. Mater.* 1 (1972) 310.
3. M. F. EHMAN, *J. Electrochem. Soc.* **121** (1974) 1240.
4. J. PAITZ and L. GOSZTONYI, in Proceedings of the European Meeting on Crystal Growth, Prague, August 1982 (Czechoslovak Scientific–Technical Society, Prague, 1982) p. 211.
5. J. H. WESTBROOK and P. J. JORGENSEN, *Trans.*

Metall. Soc. AIME **233** (1965) 425.
6. J. LANKFORD and D. L. DAVIDSON, *J. Mater. Sci.* **14** (1979) 1662.
7. A. G. EVANS and T. R. WILSHAW, *Acta Metall.* **24** (1976) 939.
8. S. HAUSSÜHL and D. MATEIKA, *Z. Naturforsch.* **27a** (1972) 1522.
9. J. LANKFORD and D. L. DAVIDSON, *J. Mater. Sci.* **14** (1979) 1669.
10. J. LANKFORD, *ibid.* **16** (1981) 1177.
11. B. R. LAWN and A. G. EVANS, *ibid.* **12** (1977) 2195.
12. A. G. EVANS and A. E. CHARLES, *J. Amer. Ceram. Soc.* **59** (1976) 371.
13. D. M. MARSCH, *Proc. Roy. Soc.* **A279** (1964) 420.
14. A. KELLY, "Strong Solids" (Clarendon Press, Oxford, 1966).
15. K. NIIHARA, R. MORENA and D. P. H. HASSELMAN, *J. Mater. Sci. Lett.* **1** (1982) 13.
16. J. LANKFORD, *ibid.* **1** (1982) 493.

Received 3 May
and accepted 21 July 1983